Herpes simplex virus-1 evasion of CD8+ T cell accumulation contributes to viral encephalitis

Naoto Koyanagi,[1,2] Takahiko Imai,[1,2] Keiko Shindo,[1,2] Ayuko Sato,[3] Wataru Fujii,[4] Takeshi Ichinohe,[2] Naoki Takemura,[5,6] Shigeru Kakuta,[7] Satoshi Uematsu,[5,6] Hiroshi Kiyono,[3,5,8] Yuhei Maruzuru,[1,2] Jun Arii,[1,2] Akihisa Kato,[1,2] and Yasushi Kawaguchi[1,2]

[1]Division of Molecular Virology, Department of Microbiology and Immunology, [2]Department of Infectious Disease Control, International Research Center for Infectious Diseases, and [3]Division of Mucosal Immunology, Department of Microbiology and Immunology, The Institute of Medical Science, The University of Tokyo, Tokyo, Japan. [4]Department of Animal Resource Sciences, Graduate School of Agricultural and Life Sciences, The University of Tokyo, Tokyo, Japan. [5]International Research and Development Center for Mucosal Vaccines, The Institute of Medical Science, The University of Tokyo, Tokyo, Japan. [6]Department of Mucosal Immunology, School of Medicine, Chiba University, Chiba, Japan. [7]Department of Biomedical Science, Graduate School of Agricultural and Life Sciences, The University of Tokyo, Tokyo, Japan. [8]Core Research for Evolutional Science and Technology, Japan Science and Technology Agency, Tokyo, Japan.

Herpes simplex virus–1 (HSV-1) is the most common cause of sporadic viral encephalitis, which can be lethal or result in severe neurological defects even with antiviral therapy. While HSV-1 causes encephalitis in spite of HSV-1–specific humoral and cellular immunity, the mechanism by which HSV-1 evades the immune system in the central nervous system (CNS) remains unknown. Here we describe a strategy by which HSV-1 avoids immune targeting in the CNS. The HSV-1 UL13 kinase promotes evasion of HSV-1–specific CD8+ T cell accumulation in infection sites by downregulating expression of the CD8+ T cell attractant chemokine CXCL9 in the CNS of infected mice, leading to increased HSV-1 mortality due to encephalitis. Direct injection of CXCL9 into the CNS infection site enhanced HSV-1–specific CD8+ T cell accumulation, leading to marked improvements in the survival of infected mice. This previously uncharacterized strategy for HSV-1 evasion of CD8+ T cell accumulation in the CNS has important implications for understanding the pathogenesis and clinical treatment of HSV-1 encephalitis.

Introduction

HSV-1 is generally associated with various mucocutaneous diseases, such as herpes labialis, genital herpes, herpetic whitlow, and keratitis (1). Also, HSV-1 is the most common cause of sporadic viral encephalitis, which can be lethal or result in severe neurological defects in a significant fraction of survivors even with antiviral therapy (2). Following primary infection at peripheral mucosal sites, HSV-1 is transported via innervating sensory neurons to replicate in sensory ganglia, such as trigeminal ganglia (TGs), and establishes lifelong latency there. HSV-1 periodically reactivates to cause lesions at or near the primary infection site, and sometimes spreads from TGs into the brain and causes encephalitis upon primary and recurrent infection (1). This HSV-1 life cycle, which repeatedly primes the host immune system, increases the potential for a host immune response to eradicate the virus, and therefore, it has been thought that HSV-1 must have evolved multiple mechanisms for evasion of immune detection and clearance, especially adaptive immune responses.

CD8+ T cells eliminate virus-infected cells through recognition of virus-derived peptides displayed at the cell surface of infected cells in the context of major histocompatibility complex class I (MHC-I) molecules (3, 4). Therefore, the MHC-I antigen presentation pathway appears to be a prime target for attack by many viruses to evade CD8+ T cells. In fact, HSV-1 has been shown to encode two viral proteins, ICP47 and Us3, both of which inhibit MHC-I antigen presentation in HSV-1–infected cells by downregulating cell surface expression of MHC-I in cell cultures (5–8). Although Us3-mediated inhibition of MHC-I antigen presentation has been reported to promote viral replication at peripheral sites in mice following footpad infection (8), whether Us3-mediated inhibition of MHC-I antigen presentation is involved in HSV-1 pathogenesis remains to be elucidated. Moreover, the role(s) of ICP47-mediated inhibition of MHC-I antigen presentation in vivo are not known, since ICP47 functioned in human cells but not in murine cells (6, 9), which makes it difficult to address the relevance of ICP47-mediated inhibition of MHC-I antigen presentation in mouse models of HSV-1 infection. Thus, data showing the significance of HSV-1 evasion of CD8+ T cells in HSV-1 replication and pathogenesis in vivo have been limited. In particular, there is a lack of information on how HSV-1 evades CD8+ T cells in the CNS, although CD8+ T cells have been suggested to play a role in clearance of HSV-1 from the CNS of infected mice (10).

UL13 is an HSV-1–encoded serine/threonine protein kinase that is conserved in members of all three subfamilies (Alphaherpesvirinae, Betaherpesvirinae, and Gammaherpesvirinae) of the family Herpesviridae (1). Although UL13 has been suggested to promote viral replication and expression of a subset of viral genes in cell cultures in a manner dependent on the cell type and to potentially mimic cellular cyclin-dependent protein kinases (11–15), the role(s) of UL13 in viral replication and pathogenicity in vivo have remained unknown. Here we showed that UL13 kinase promoted evasion of HSV-1–specific CD8+ T cell accumulation by downregulating expression of CXCL9 within the CNS and that this UL13-mediated evasion of CD8+ T cells was critical for mortality due to viral encephalitis.

Conflict of interest: The authors have declared that no conflict of interest exists.
Submitted: January 19, 2017; **Accepted:** July 26, 2017.
Reference information: *J Clin Invest.* 2017;127(10):3784–3795.
https://doi.org/10.1172/JCI92931.

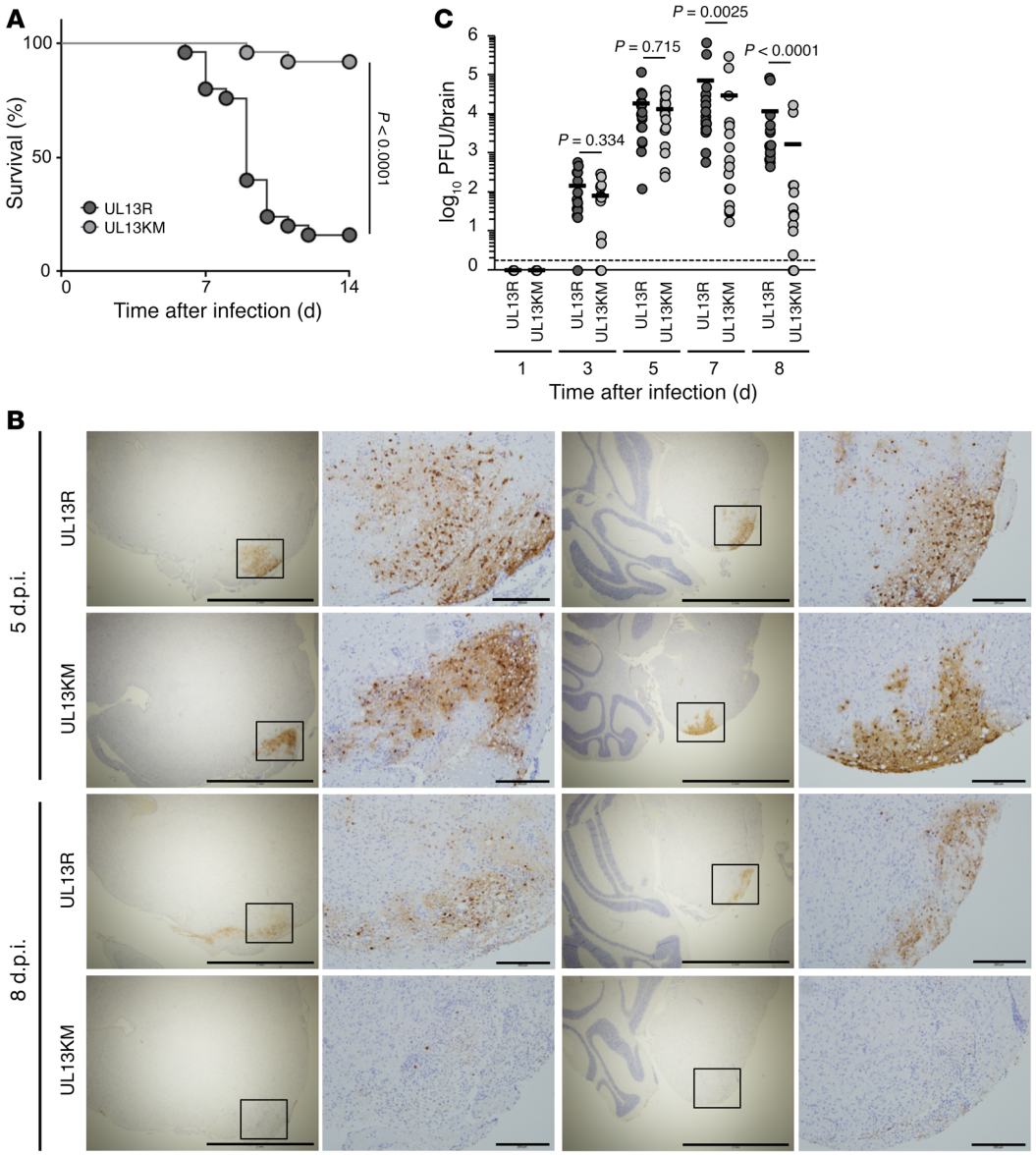

Figure 1. Effect of HSV-1 UL13 kinase activity on viral replication and pathogenicity in the CNS of mice following ocular infection. (**A**) Five-week-old female ICR mice were ocularly infected with 1×10^6 PFU UL13KM or UL13R per eye and monitored for survival daily for 14 days. The results of 3 independent experiments (1 with 5 mice and 2 with 10 mice) were combined. (**B**) At 5 and 8 days after infection, the brains of infected mice were harvested, sectioned, stained with an antibody to HSV-1 antigens, and analyzed by fluorescence microscopy. In each row, the first and third images are of different sections, and the second and fourth images are higher magnifications of the boxed areas of the sections in the first and third images, respectively. Magnification of first and third images, 4× objective lens. Scale bars: 2 mm. Magnification of second and fourth images, 20× objective lens. Scale bars: 200 μm. d.p.i., day(s) after infection. (**C**) Viral titers in the brains of infected mice at 1, 3, 5, 7, and 8 days after infection were assayed. Dashed line indicates the limit of detection. The results of 3 independent experiments (1 with 7 mice and 2 with 5 mice) were combined for each virus. Each data point is the virus titer in the brain of one mouse. Statistical significance values were analyzed by the log-rank test (**A**) or the Mann-Whitney *U* test (**C**).

Results

Effect of UL13 kinase activity on HSV-1 replication in the CNS and pathogenicity in mice. In experimental murine models of HSV-1 infection, the capacity to invade the CNS from peripheral sites, such as eye and vagina, and to damage the CNS due to viral replication can be studied in mice following peripheral inoculation (e.g., ocular and vaginal) (16). In these murine models, mortality results from HSV-1 encephalitis caused by viral CNS infection (1, 17). To clarify the role(s) of UL13 kinase activity in viral replication in the CNS and in viral pathogenicity, we ocularly infected mice with a recombinant HSV-1 (UL13KM) carrying a K176M mutation in UL13, which was reported to inactivate UL13 kinase activity without affecting expression of UL13 protein (18), or a recombinant HSV-1 (UL13R) in which the K176M mutation in UL13KM was repaired (Supplemental Figure 1; supplemental material available online with this article; https://doi.org/10.1172/JCI92931DS1), and monitored survival. Notably, most (92.0%) UL13KM-infected mice survived, but most (84.0%) UL13R-infected mice died (Figure 1A). Furthermore, at 5 days after infection, HSV-1 antigens in the brain stems, which are the predominant infection sites following ocular

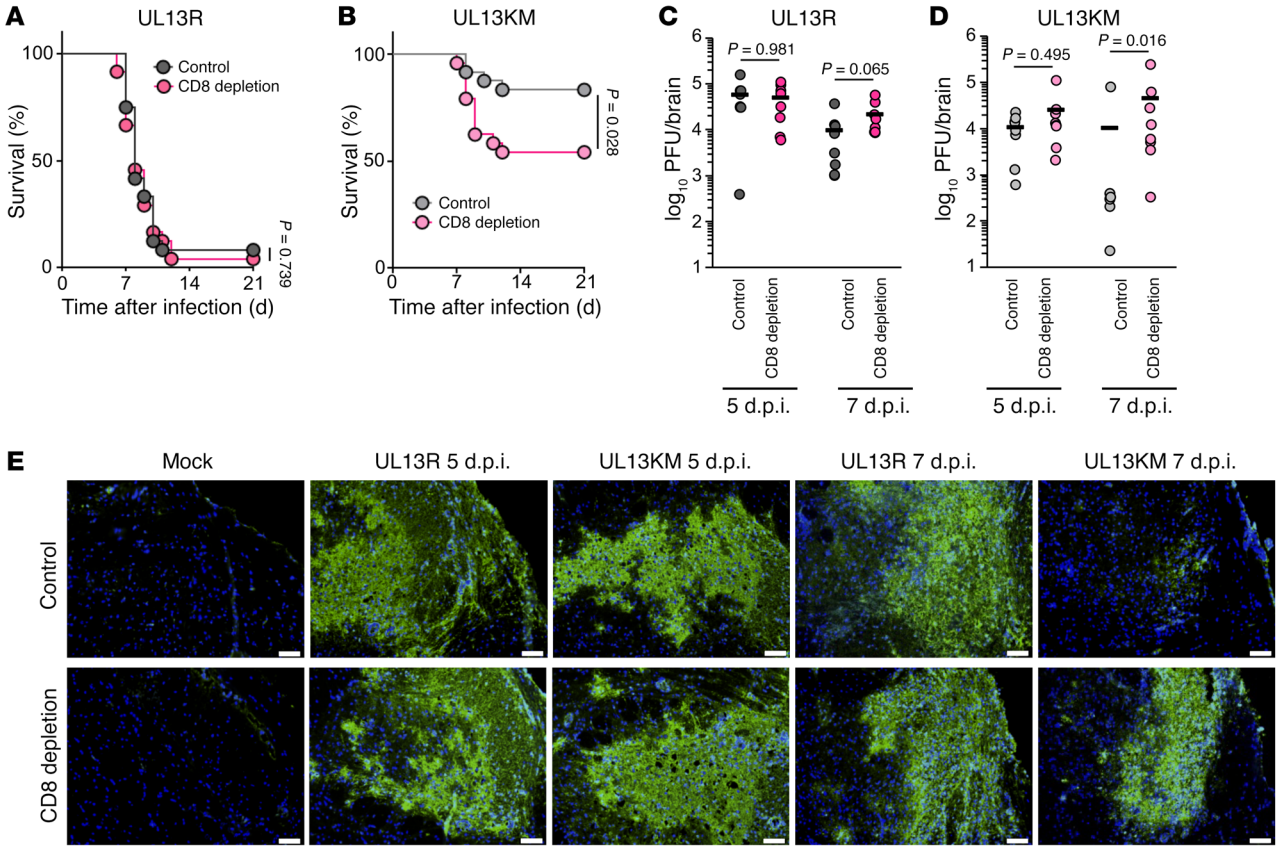

Figure 2. Effect of depletion of CD8⁺ T cells on replication and pathogenicity of HSV-1 with and without UL13 kinase activity in the brains of mice following ocular infection. (**A** and **B**) Five-week-old female ICR mice mock-depleted or CD8⁺ T cell–depleted were mock-infected or infected with 1×10^6 PFU UL13R (**A**) or UL13KM (**B**) per eye and monitored for survival daily for 21 days. The results from 2 independent experiments (each with 12 mice) were combined. The statistical significance values were analyzed by the log-rank test. (**C** and **D**) At 5 and 7 days after infection, viral titers in the brains of mice infected with UL13R (**C**) or UL13KM (**D**) were assayed. The results from 2 independent experiments (each with 4 mice) were combined. Each data point is the virus titer in the brain of one mouse. The statistical significance values were analyzed by the Mann-Whitney *U* test. (**E**) At 5 and 7 days after infection, the brains of infected mice were harvested, sectioned, stained with an antibody to HSV-1 antigens, and analyzed by fluorescence microscopy. Magnification of images, 20× objective lens. Scale bars: 50 μm.

inoculation (19), were similarly detected in almost all mice infected with UL13KM and UL13R (Figure 1B). In contrast, at 8 days after infection, HSV-1 antigens were detected in almost all UL13R-infected mice but were barely detectable in UL13KM-infected mice (Figure 1B). However, HSV-1 antigens in brain stems were only detected in a fraction of UL13KM-infected mice, at a level similar to that in UL13R-infected mice (data not shown). Accordingly, the titer of UL13KM in the brains was similar to that of UL13R at 3 and 5 days after infection (Figure 1C). However, the UL13KM titer was significantly lower than that of UL13R at 7 and 8 days after infection (Figure 1C). These results suggested that UL13 kinase activity was required for efficient evasion of viral clearance in the CNS and effective HSV-1 mortality in mice following ocular infection.

Effect of CD8⁺ T cells on viral virulence and replication in the CNS of mice following ocular inoculation. It has been reported that CD8⁺ T cells play a role in the clearance of HSV-1–infected cells in the brains of mice following ocular inoculation (10). Therefore, to investigate whether CD8⁺ T cells contributed to clearance of infected cells in the brains as shown in Figure 1, B and C, we infected mice injected with CD8-depleting or CD4-depleting antibodies with UL13KM or UL13R. CD8⁺ T cell depletion significantly decreased survival of UL13KM-infected mice but had no effect on lethality of UL13R-infected mice (Figure 2, A and B). In contrast, CD4⁺ T cell depletion had no effect on survival of UL13KM-infected mice, although it slightly enhanced lethality of UL13R-infected mice (Supplemental Figure 2). At 5 days after infection, CD8⁺ T cell depletion had no effect on viral replication or antigen spread in the brains of UL13KM-infected and UL13R-infected mice (Figure 2, C–E). However, at 7 days after infection, depletion of CD8⁺ T cells significantly increased viral replication and antigen spread in UL13KM-infected mice, but not in UL13R-infected mice (Figure 2, C–E), indicating that CD8⁺ T cells were required for efficient clearance of UL13KM-infected cells and for efficient survival. Thus, UL13 kinase activity likely promoted evasion of CD8⁺ T cells but not CD4⁺ T cells in the CNS, which appeared to be critical for mortality due to HSV-1 encephalitis.

Effect of UL13 kinase activity on regulation of HSV-1–specific CD8⁺ T cell accumulation in the CNS. We then investigated two mechanisms by which UL13 kinase activity might promote viral evasion of CD8⁺ T cells in the CNS: UL13 kinase activity might inhibit CD8⁺ T cell accumulation in the CNS, or UL13 kinase activity might downregulate antigen presentation in HSV-1–infected

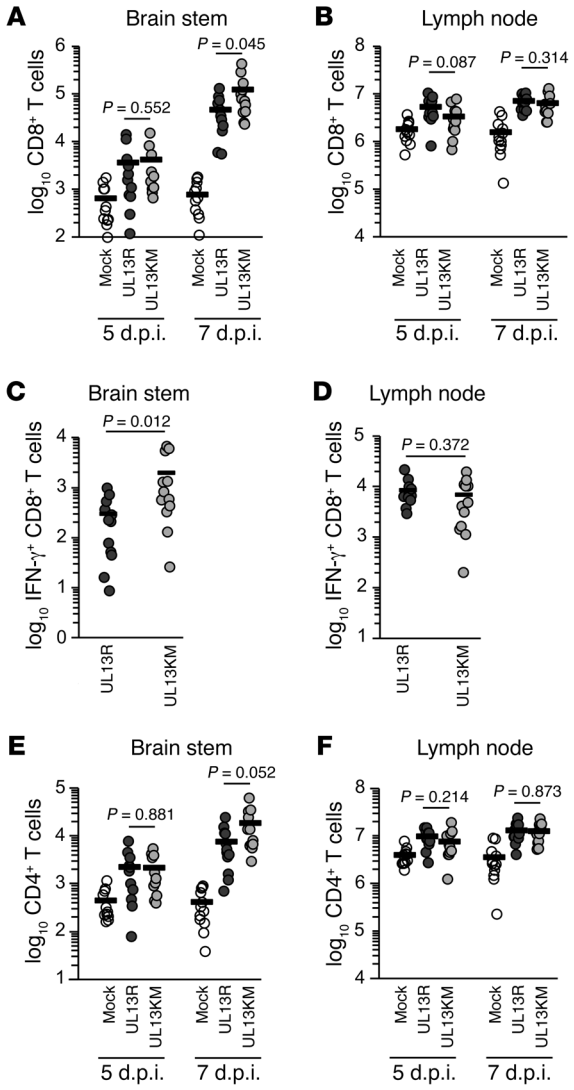

Figure 3. Effect of HSV-1 UL13 kinase activity on the accumulation of CD8⁺ T cells in the infected brain stems of mice following ocular infection. (**A**, **B**, **E**, and **F**) Five-week-old female ICR mice were mock-infected or infected with 1×10^6 PFU UL13R or UL13KM per eye. At 5 or 7 days after infection, brain stem (**A** and **E**) and submandibular lymph node (**B** and **F**) samples were processed and analyzed for CD8⁺ T (CD8⁺, CD3⁺, and CD45⁺) (**A** and **B**) or CD4⁺ T (CD4⁺, CD3⁺, and CD45⁺) (**E** and **F**) cell content by flow cytometry. The results from 3 independent experiments (1 with 3 mice and 2 with 4 mice for the 5 days post-infection experiments, and 3 with 4 mice for the 7 days post-infection experiments) were combined. Each data point is the number of CD8⁺ or CD4⁺ T cells in the brain stem (**A** and **E**) or submandibular lymph node (**B** and **F**) of one mouse. (**C** and **D**) At 7 days after infection, CD8⁺ T cells purified from brain stem (**C**) and submandibular lymph node samples (**D**) were assayed for the number of IFN-γ–producing cells by ELISPOT assays. The results from 3 independent experiments (each with 4 mice) were combined. Each data point is the number of IFN-γ–producing CD8⁺ T cells in the brain stem (**C**) or submandibular lymph node (**D**) of one mouse. Statistical significance values were analyzed by the Mann-Whitney *U* test.

cells, as reported for ICP47 and Us3 (6–8). First, we examined the effect of UL13 kinase activity on CD8⁺ T cell accumulation in the brain. The number of CD8⁺ T cells was similar in the brain stems of mice infected with UL13KM or UL13R at 5 days after infection, but was significantly greater in the brain stems of mice infected with UL13KM compared with UL13R at 7 days after infection (Figure 3A). CD8⁺ T cells were then isolated from the brain stems and submandibular lymph nodes of UL13KM- and UL13R-infected mice and restimulated ex vivo with HSV-1 antigens, and the number of IFN-γ–secreting cells was analyzed by enzyme-linked immunosorbent spot (ELISPOT) assays. There were significantly more HSV-1–specific IFN-γ⁺CD8⁺ T cells in the brain stems of UL13KM-infected mice than in UL13R-infected mice (Figure 3C). Meanwhile, the number of total or HSV-1–specific CD8⁺ T cells was similar in submandibular lymph nodes of mice infected with UL13KM or UL13R (Figure 3, B and D). These results suggested that UL13 kinase activity was required for efficient evasion of HSV-1–specific CD8⁺ T cell accumulation in the brain stems of mice following ocular infection. Next, we examined the effect of UL13 kinase activity on HSV-1–specific antigen presentation in HSV-1–infected cells using a cytotoxic T lymphocyte (CTL) hybridoma clone that produced β-galactosidase in response to the immunodominant $gB_{498-505}$ epitope of HSV-1 (20). As we reported previously (8), the response of HSV-1–specific CTL hybridoma clone to cells infected with a recombinant HSV-1 lacking Us3 (ΔUs3) (Supplemental Figure 1) was significantly greater than with WT HSV-1(F) or with a recombinant virus (ΔUs3R) in which the Us3-null mutation in ΔUs3 was repaired. In contrast, the response of the HSV-1–specific CTL hybridoma clone to cells infected with UL13KM was similar to that of cells infected with WT HSV-1(F) or UL13R (Supplemental Figure 3), suggesting that UL13 kinase activity played no apparent role in the inhibition of MHC class I–restricted, HSV-1–specific antigen presentation in HSV-1–infected cells.

Effect of UL13 kinase activity on HSV-1 replication and CD8⁺ T cell accumulation at the peripheral sites. We examined the effect of UL13 kinase activity on viral replication and CD8⁺ T cell accumulation in peripheral sites including the eyes and TGs of mice following ocular infection with UL13KM or UL13R. As shown in Figure 4A, the titer of UL13KM in eyes was similar to that of UL13R at 1 day after infection, whereas the UL13KM titer was significantly lower than that of UL13R at 3, 5, 7, and 8 days after infection. In TGs, the titer of UL13KM was similar to that of UL13R at 3 and 5 days after infection, whereas the UL13KM titer was significantly lower than that of UL13R at 7 and 8 days after infection (Figure 4C). Thus, as observed in the brain, the UL13KM titer was initially similar to that of UL13R in eyes and TGs, and was significantly lower than the UL13R titer thereafter, although the differences in viral titers between UL13KM and UL13R were detectable earlier in eyes (at 3 days after infection) (Figure 4A) and TGs (at 5 days after infection) (Figure 4C) than in brains (at 7 days after infection) (Figure 1C). In contrast, the number of CD8⁺ T cells was similar in the eyes and TGs of mice infected with UL13KM or UL13R at 5 and 7 days after infection (Figure 4, B and D), unlike in the CNS of mice infected with UL13KM or UL13R (Figure 3A). These results indicated that although UL13 kinase activity was required for efficient HSV-1 replication in peripheral and central sites, it was required for the efficient inhibition of accumulation of CD8⁺ T cells in the CNS only and not in the peripheral sites.

Effect of UL13 kinase activity on induction of cytokines in HSV-1 infection sites in the CNS. CD8⁺ T cell attractant chemokines CXCL9,

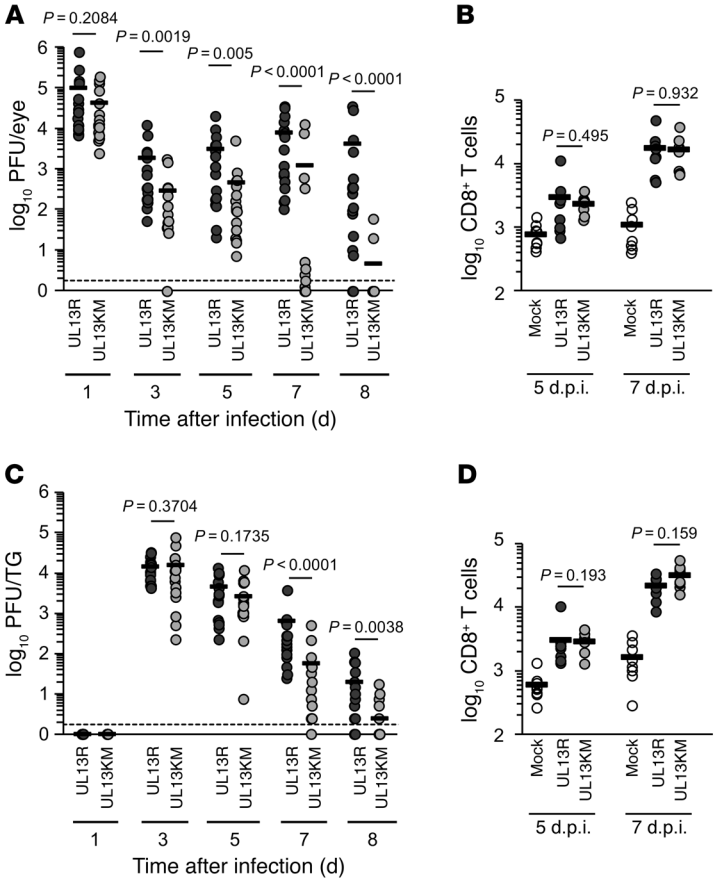

Figure 4. Effect of HSV-1 UL13 kinase activity on viral replication and accumulation of CD8⁺ T cells in the eye and TGs of mice following ocular infection. Five-week-old female ICR mice were mock-infected or ocularly infected with 1×10^6 PFU UL13KM or UL13R per eye. (**A** and **C**) At 1, 3, 5, 7, and 8 days after infection, eye and TG samples were processed, and viral titers in the eyes (**A**) or the TGs (**C**) of infected mice were assayed. Dashed line indicates the limit of detection. The results of 3 independent experiments (1 with 7 mice and 2 with 5 mice) were combined for each virus. Each data point is the virus titer in the eye (**A**) or the TGs (**C**) of one mouse. (**B** and **D**) At 5 or 7 days after infection, eye (**B**) and TG (**D**) samples were processed and analyzed for CD8⁺ T (CD8⁺, CD3⁺, and CD45⁺) cell content by flow cytometry. The results from 2 independent experiments (each with 4 mice) were combined. Each data point is the number of CD8⁺ T cells in the eyes (**B**) or TGs (**D**) of one mouse. The statistical significance values were analyzed by the Mann-Whitney *U* test.

CXCL10, and CXCL11 use CXCR3, which is highly expressed on activated T cells, as a receptor (21), and CXCL9 and CXCL10 have been reported to recruit HSV-specific CD8⁺ T cells to HSV infection sites (22). Therefore, we compared expression of these chemokines and IL-6 in the brain stems of mice infected with UL13KM or UL13R. The level of *Cxcl9* mRNA expression was not significantly different in the brain stems of mice infected with UL13KM or UL13R at 5 days after infection (data not shown), but was significantly higher in the brain stems of mice infected with UL13KM than in mice infected with UL13R at 7 days after infection (Figure 5A). In contrast, the levels of mRNA expression of *Cxcl10*, *Cxcl11*, and *IL-6* in the brain stems of mice infected with UL13KM were similar to those in mice infected with UL13R (Figure 5, B–D). These results indicated that UL13 kinase activity was required for the efficient downregulation of CXCL9 expression in the brain stems, and that the UL13-mediated downregulation of CXCL9 might inhibit the accumulation of HSV-1–specific CD8⁺ T cells in the brain stem. In support of this hypothesis, although there were similar numbers of CD4⁺ T cells, which are known to be recruited to HSV-1 infection sites by CXCL9 (23), in the brain stems of UL13KM- and UL13R-infected mice at 5 days after infection, there was a tendency toward greater numbers of CD4⁺ T cells in the brain stems of UL13KM-infected mice compared with UL13R-infected mice at 7 days after infection (Figure 3E). As observed with CD8⁺ T cells, the number of CD4⁺ T cells in submandibular lymph nodes of UL13KM-infected mice was similar to that in UL13R-infected mice (Figure 3F).

Effect of injection of CXCL9 in HSV-1 infection sites in the CNS on viral replication and pathogenicity. To address more directly the hypothesis that UL13-mediated downregulation of CXCL9 inhibited the accumulation of HSV-1–specific CD8⁺ T cells in the brain stems of infected mice and enabled efficient viral replication and virulence, we investigated whether injection of CXCL9 into the brain stems of mice infected with UL13R — which downregulated expression of CXCL9 in brain stems as shown above — induced the phenotype observed in mice infected with UL13KM, including the increase in the accumulation of HSV-1–specific CD8⁺ T cells in the brain stems and the decrease in viral replication in the brains and in mortality of infected mice. For these experiments, mice ocularly infected with UL13R were mock-injected or injected stereotaxically with CXCL9 into brain stems at 5 days after infection. As shown in Figure 6, A–D, direct CXCL9 injection into the brain stems of UL13R-infected mice significantly increased the total number of CD8⁺ T cells and the number of HSV-1–specific IFN-γ⁺CD8⁺ T cells accumulated in the brain stems, but CXCL9 injection had no significant effect on the number of these cells in the submandibular lymph nodes of infected mice at 7 days after infection. Similar experiments on CD4⁺ T cell accumulation showed that CXCL9 injection tended to induce the accumulation of CD4⁺ T cells in the brain stems of infected mice, but had no effect on the number of these cells in submandibular lymph nodes of infected mice at 7 days after infection (Figure 6, E and F). Furthermore, CXCL9 injection significantly reduced viral replication in the brains and mortality (Figure 6, G and H). Notably, direct injection of CXCL10, which is a redundant chemokine of CXCL9 and shares its receptor CXCR3 with CXCL9, induced the same effects as CXCL9 (Supplemental Figure 4). These results indicated that CXCL9 and CXCL10 were able to accumulate HSV-1–specific CD8⁺ T cells at infection sites in the CNS, and overexpression of CXCL9 or CXCL10 in the infection sites reduced viral replication in these sites and mortality of infected mice by a pathway common to CXCL9 and CXCL10.

The CXCL9 and CXCL10 receptor CXCR3 is expressed on many cell types other than CD8⁺ and CD4⁺ T cells, such as NK cells, NKT cells, plasmacytoid DCs, subsets of B cells, neutrophils, microglia, astrocytes, and neurons (21, 24–27). Therefore, for investigation of whether the effects of CXCL9 injection were dependent on CD8⁺ T cells, mice injected with CD8-depleting antibody were infected with UL13R and then were mock-injected or injected with

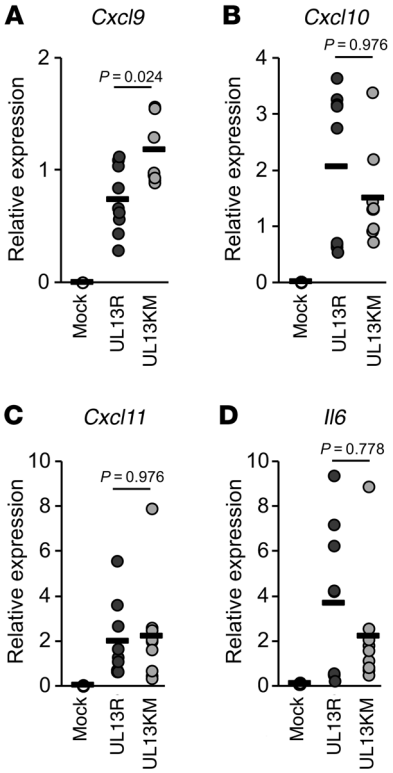

Figure 5. Effect of HSV-1 UL13 kinase activity on expression of cytokine mRNAs in the infected brain stems of mice following ocular infection. Five-week-old female ICR mice were mock-infected or infected with 1×10^6 PFU UL13R or UL13KM per eye. At 7 days after infection, brain stem samples were processed, and the amounts of *Cxcl9* (**A**), *Cxcl10* (**B**), *Cxcl11* (**C**), and *Il-6* (**D**) mRNA were analyzed by quantitative RT-PCR. The results from 2 independent experiments (1 with 4 mice and 1 with 5 mice) were combined. Each data point is the relative amount of each mRNA in the brain stem of one mouse. The statistical significance values were analyzed by the Mann-Whitney *U* test.

CXCL9 into brain stems at 5 days after infection. As shown in Figure 7, A and B, CXCL9 injection had no significant effect on viral replication or the mortality of CD8-depleted mice in contrast to normal mice injected with CXCL9 (Figure 6, G and H). These results eliminated the possibility that the CXCL9 injection was acting through cell types other than $CD8^+$ T cells expressing CXCR3.

Thus, direct injection of CXCL9 into the brain stems of mice infected with UL13R produced a phenotype similar to the UL13 kinase-dead mutation that was dependent on $CD8^+$ T cells. These results supported our hypothesis that UL13 kinase activity promoted downregulation of CXCL9 to evade the accumulation of HSV-1–specific $CD8^+$ T cells in the infection site in the CNS, enabling efficient viral replication and pathogenicity in the mouse CNS.

Effect of CXCL9 knockout on HSV-1 pathogenicity in mice. Finally, we examined the effect of CXCL9 knockout in mice infected with HSV-1. We generated *Cxcl9*-knockout mice with a 45-bp deletion in the target region of the *Cxcl9* gene (Supplemental Figure 5A) by the offset-nicking method of the CRISPR/Cas system as previously described (28). Primary mouse embryonic fibroblasts (MEFs) from WT or homozygotic *Cxcl9*-knockout mice were mock-treated or treated with recombinant murine IFN-γ and tested for the expression of CXCL9 protein by immunoblotting. As shown in Supplemental Figure 5B, IFN-γ–dependent CXCL9 expression was observed in MEFs from WT mice but not from *Cxcl9*-knockout mice, confirming the generation of *Cxcl9*-knockout mice. Then, WT or *Cxcl9*-knockout mice were infected with UL13KM or UL13R, and their survival was monitored. As shown in Supplemental Figure 5C, the survival rate of *Cxcl9*-knockout mice was significantly greater than that of WT mice following ocular infection with UL13R. In contrast, the survival rate of *Cxcl9*-knockout mice was similar to that of WT mice following ocular infection with UL13KM (Supplemental Figure 5D). These results indicated that CXCL9 was required for efficient viral virulence in mice following ocular infection and that the complete depletion of CXCL9 could not enhance the virulence of HSV-1 UL13KM in contrast to $CD8^+$ T cell depletion (Figure 2B).

Discussion

It has been reported that topical CXCL9 and CXCL10 administration in the genital tract of mice that had been vaccinated with an attenuated recombinant HSV lacking the thymidine kinase gene significantly increased recruitment of HSV-specific $CD8^+$ T cells to the infection site and protected the mice against lethal genital HSV challenge (22). In this study, we showed that the ocular inoculation of UL13R into mice induced the expressions of CXCL9 and CXCL10 in the CNS. Of note, most of the UL13R-infected mice died, suggesting that although CXCL9 and CXCL10 reduce HSV infection by recruiting HSV-specific $CD8^+$ T cells to the infection sites, this was insufficient to block infection, thereby enabling efficient viral replication and pathogenicity. Therefore, HSV might have evolved mechanism(s) to downregulate the effect of CXCL9 and/or CXCL10 at infection sites. In agreement with this hypothesis, we have presented data here suggesting that HSV-1 protein kinase UL13 mediated downregulation of CXCL9 expression to inhibit the accumulation of HSV-1–specific $CD8^+$ T cells at infection sites in the CNS of mice, allowing efficient viral replication and pathogenicity. This conclusion was supported by the findings of several reported studies as follows: (i) delayed infiltration of HSV-1–specific $CD8^+$ T cells into the CNS in mice, caused by psychological stress, was shown to promote viral encephalitis (29); (ii) accumulating evidence has suggested the involvement of various chemokines in the immunopathogenesis of other infectious diseases in the CNS (30); and (iii) various herpesviruses encode chemokine homologs, chemokine receptor homologs, and/or chemokine-binding proteins as part of multiple strategies to regulate chemokines (31). To the best of our knowledge, this is the first report of an HSV strategy for $CD8^+$ T cell evasion that regulates HSV-1 pathogenesis and is employed in the CNS. Since HSV-1 UL13 is conserved in herpesviruses in all three Herpesviridae subfamilies, the HSV-1 UL13–mediated immune evasion mechanism may be conserved in other herpesviruses, especially in neurotropic herpesviruses subclassified in the Alphaherpesvirinae subfamily, such as varicella-zoster virus, pseudorabies virus, and equine herpesvirus, which sometimes cause encephalitis (32). At present, whether Us3 and ICP47, which have been reported to downregulate HSV-1–specific MHC-I antigen presentation (5, 6, 8, 9), function in $CD8^+$ T cell evasion in the CNS remains to be investigated. However, it is likely that the mul-

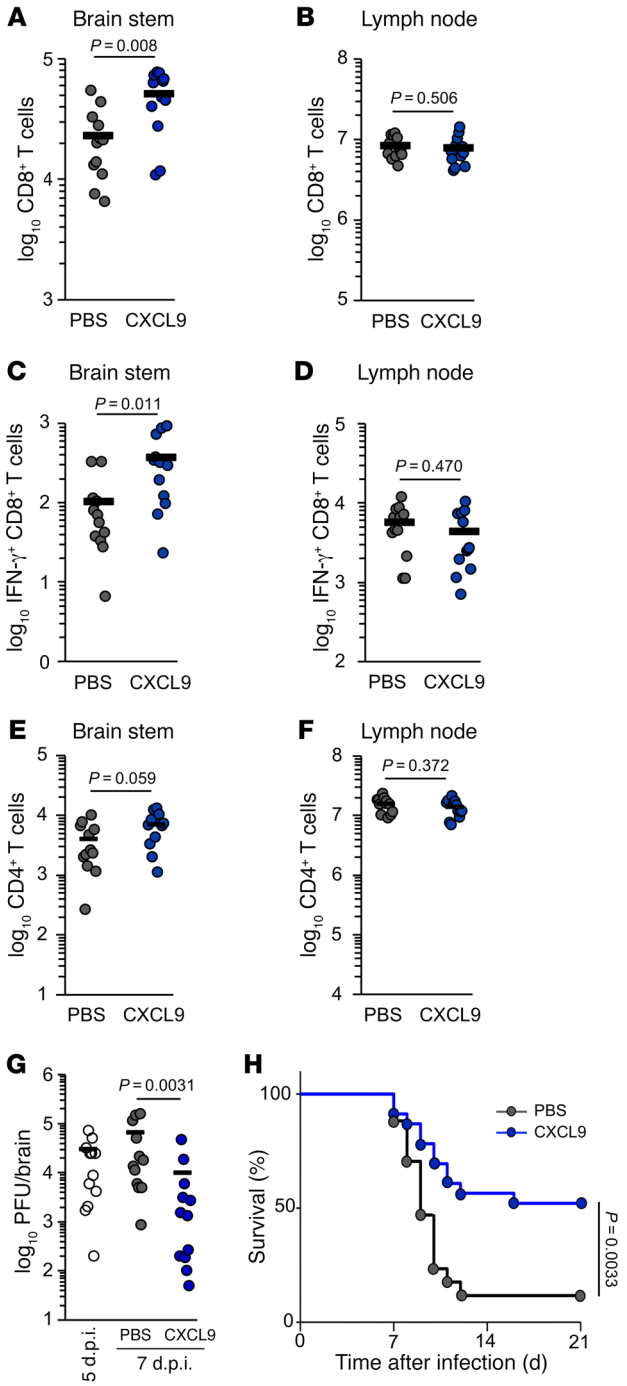

Figure 6. Effect of direct injection of CXCL9 into the brain stems of mice ocularly infected with UL13R on CD8⁺ T cell accumulation and viral pathogenicity. (**A**–**G**) Five-week-old female ICR mice were ocularly infected with 1×10^6 PFU UL13R per eye. At 5 days after infection, CXCL9 or PBS was injected into the brain stems of the infected mice. At 7 days after infection, brain stem (**A** and **E**) and submandibular lymph node (**B** and **F**) samples were processed and analyzed for CD8⁺ T (CD8⁺, CD3⁺, and CD45⁺) (**A** and **B**) or CD4⁺ T (CD4⁺, CD3⁺, and CD45⁺) (**E** and **F**) cell content by flow cytometry. At 7 days after infection, CD8⁺ T cells purified from brain stem (**C**) and submandibular lymph node samples (**D**) were assayed for IFN-γ–producing cell content by ELISPOT assays. At 5 and 7 days after infection, viral titers in the brains of infected mice were assayed (**G**). The results from 3 independent experiments (each with 4 mice) were combined. Each data point is the number of each type of cells in each tissue of one mouse (**A**–**F**) or the virus titer in the brain of one mouse (**G**). (**H**) Survival was monitored daily for 21 days. The results from 4 independent experiments (1 with 5 mice and 3 with 6 mice for the CXCL9 injection experiments; and 1 with 3 mice, 1 with 4 mice, and 2 with 5 mice for the PBS injection experiments) were combined. The statistical significance values were analyzed by the Mann-Whitney *U* test (**A**–**G**) or the log-rank test (**H**).

tiple mechanisms for CD8⁺ T cell evasion promoted by UL13, Us3, and ICP47 may be critical for viral replication and pathogenicity in the mouse CNS. We observed an increased accumulation of CD8⁺ T cells in the CNS but not in the eyes and TGs of UL13KM-infected mice, indicating the HSV-1 UL13–mediated immune evasion mechanism might be specific to the CNS. However, we cannot eliminate the possibility that it might also function in peripheral infection sites to enable efficient viral replication and pathogenicity, probably in concert with Us3 and ICP47.

The importance of CD4⁺ T cells in control of HSV infection has been reported (33–36). Notably, we showed here that CD4⁺ T cell depletion had no obvious effect on lethality of UL13R- and UL13KM-infected mice. These results suggested that CD4⁺ T cells played no obvious roles in prevention of lethality in mice following ocular HSV-1 infection and appear not to be in agreement with the previous reports. As described above, ICP47, a strong inhibitor of HSV-1–specific MHC-I antigen presentation, does not function in murine cells (6, 9). Therefore, the CD8⁺ T cell response to HSV infection could be exaggerated in mouse models due to the dysfunction of ICP47, and this may lead to underestimation of the importance of CD4⁺ T cells in control of HSV infection in mouse models.

It is interesting that HSV-1 UL13 downregulated CXCL9 but not its redundant chemokine CXCL10 in the CNS in mice. A non-redundant role for CXCL9 and CXCL10 in the immune response to HSV-1 ocular infection has been reported, with CXCL9 but not CXCL10 playing an important role in recruitment of CD4⁺ T cells into the cornea in mice following HSV-1 ocular infection (23). Similarly, CXCL9 may have a specific role and/or potential in recruitment of CD8⁺ T cells into the CNS in mice, and therefore, HSV-1 UL13 may target only CXCL9, although the current study showed that the excessive administration of either CXCL9 or CXC10 promoted the accumulation of CD8⁺ T cells into the CNS. This specific UL13-mediated downregulation of CXCL9 also eliminates the possibility that the increase in CXCL9 expression in the absence of UL13 shown in this study resulted from reduced activity of the virus endoribonuclease responsible for viral host protein synthesis shutoff (vhs). In agreement with this, we showed that the absence of UL13 kinase activity had no effect on the activity of vhs protein in infected cells (Supplemental Figure 6, A and B), although vhs protein has been reported to be phosphorylated by UL13 (37). At present, the mechanism by which UL13 downregulates CXCL9 expression in the CNS remains unknown. Whereas UL13 may play a direct role in suppression of CXCL9 gene expression, there is also the possibilities that UL13 indirectly regulates CXCL9 gene expression by downregulating expression of IFN-γ, which induces CXCL9 gene expression (21), in infected cells and/or by downregulating infiltration of immune cells secreting IFN-γ into the infection sites.

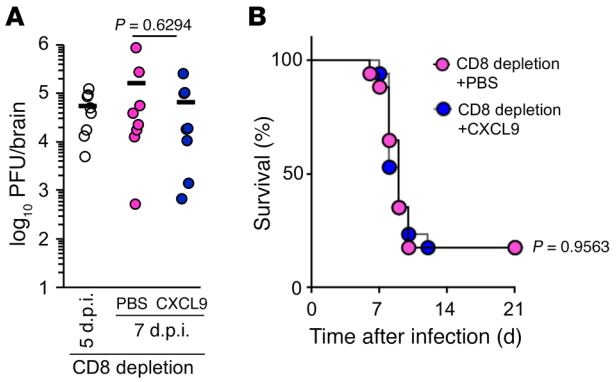

Figure 7. Effect on viral pathogenicity of direct injection of CXCL9 into the brain stems of mice depleted of CD8⁺ T cells and ocularly infected with UL13R. Five-week-old female ICR mice depleted of CD8⁺ T cells were infected with 1×10^6 PFU UL13R per eye. At 5 days after infection, CXCL9 or PBS was injected into the brain stems of the infected mice. (**A**) At 5 and 7 days after infection, viral titers in the brains of infected mice were assayed. The results from 2 independent experiments (each with 4 mice) were combined. Each data point is the virus titer in the brain of one mouse. (**B**) Survival was monitored daily for 21 days. The results from 4 independent experiments (2 with 6 mice and 2 with 3 mice) were combined. The statistical significance values were analyzed by the Mann-Whitney *U* test (**A**) or the log-rank test (**B**).

Accumulating data have suggested that the dysregulation of CNS inflammatory responses by HSV-1 infection appears to be a critical determinant of the lethality of HSV-1 encephalitis (19, 38, 39). In this study, we showed that the ability of HSV-1 to downregulate CXCL9 expression and inhibit the accumulation of HSV-1–specific CD8⁺ T cells to infection sites in the CNS was correlated with an increase in viral mortality in mice. Importantly, we also showed that direct injections of CXCL9 and CXCL10 into the CNS of HSV-1–infected mice significantly increased the accumulation of HSV-1–specific CD8⁺ T cells in CNS infection sites and reduced mortality of infected mice due to encephalitis. Taken together, these observations suggested that HSV-1–specific CD8⁺ T cells infiltrated into CNS infection sites downregulated the dysregulation of the inflammatory response in the CNS, thereby leading to a significant increase in the survival of infected mice. In support of this hypothesis, artificially enhanced infiltration of West Nile virus–specific (WNV-specific) CD8⁺ T cells into the CNS in mice was reported to increase viral clearance and reduce the inflammatory response within the CNS, leading to significant improvement in survival of mice infected with a highly cytopathic strain of WNV (40). Therefore, our study may provide insight into the mechanism(s) of immunopathology in CNS infections of cytopathic viruses, which is much less clear than the immunopathology of CNS autoimmune diseases and noncytopathic viral infections of the CNS, such as multiple sclerosis and lymphocytic choriomeningitis virus infection, in which inappropriate CNS lymphocyte entry is associated with significant immunopathology (41, 42). It has been reported that once dysregulation of CNS inflammatory responses is initiated after HSV-1 infection in the CNS, inhibition of viral replication by anti-herpetic drugs (e.g., acyclovir) is not sufficient for preventing fetal HSV-1 encephalitis (2, 19), resulting in death or severe neurological defects in a significant fraction of survivors. Our results not only elucidated the mechanism of HSV-1 evasion of CD8⁺ T cells in the CNS, but also suggested a new therapeutic approach for treatment of fetal and critical HSV-1 encephalitis; i.e., artificial recruitment of HSV-1–specific CD8⁺ T cells into infection sites in the CNS may improve the prognosis of HSV-1 encephalitis. These therapeutic possibilities may include delivery or induction of CXCL9 and/or CXCL10 in the HSV-1 infection site in the CNS, or development of drugs that inhibit UL13 kinase activity.

Here, we clarified the role of CXCL9 in HSV-1–specific CD8⁺ T cell accumulation in the mouse CNS following ocular infection with HSV-1, which appeared to negatively regulate the mortality of infected mice; however, it has also been reported that CXCL9 is required for efficient HSV-1 virulence in mice following ocular infection (43). CXCL9 depletion via CXCL9-depleting antibody injection was shown to significantly increase the survival of susceptible 129S6 mice following ocular infection with WT HSV-1 (43). In agreement with this report, we demonstrated that the survival of *Cxcl9*-knockout ICR mice was significantly greater than that of WT ICR mice, following ocular infection with UL13R. CXCL9 may be necessary for the initiation of a subset of CNS inflammatory responses to HSV-1 infection, the regulation of which is critical for the lethality of HSV-1 encephalitis (43). In support of this, HSV-1 infection has been shown to induce CXCL9 expression, as shown here and in earlier studies (43). Collectively, these observations suggested that CXCL9 played opposing roles in HSV-1 virulence in the CNS, probably depending on the quantity and/or timing of CXCL9 expression during the infection, just like other cytokines such as IL-10 do in other viral infections (44, 45). Therefore, HSV-1 needs to tightly regulate CXCL9 expression, and thus has evolved to express UL13 as regulator of CXCL9. Notably, we also showed that the survival curve of CXCL9-deficient ICR mice was similar to that of WT ICR mice following ocular infection with UL13KM. Conceivably, as loss of CXCL9 did not enhance mortality in UL13KM-infected *Cxcl9*-knockout mice, a further increase in mortality mediated by precluding the negative role of CXCL9, i.e., induction of CD8+ T cell accumulation, on viral virulence, may be antagonized by the positive role of CXCL9 on viral virulence.

Methods

Cells and viruses. Vero and rabbit skin cells (gifts from Bernard Roizman, University of Chicago, Chicago, Illinois, USA), and B6MEFs (gift from Noboru Mizushima, University of Tokyo, Tokyo, Japan), an immortalized MEF cell line derived from WT C57BL/6J mice, were described previously (8, 46). HSV-2.3.2E2 cells (gift from Francis Carbone, University of Melbourne, Melbourne, Victoria, Australia) (20), a LacZ-inducible CD8⁺ T cell hybridoma that recognizes HSV-1 $gB_{498-505}$, were described previously (8). Mouse neuroblastoma Neuro-2a cells (gift from Shinobu Kitazume, RIKEN, Saitama, Japan) were maintained in DMEM containing 10% fetal calf serum. HSV-1 WT strain HSV-1(F), recombinant Us3-null mutant virus ΔUs3 (R7041), recombinant virus ΔUs3R (R7306) in which the Us3-null mutation was repaired, and recombinant UL13-null mutant virus ΔUL13 (R7356) (gifts from Bernard Roizman), recombinant UL41-null mutant virus ΔUL41 (YK476), and recombinant virus ΔUL41R (YK477) in which the UL41-null mutation was repaired were described previously (12, 13, 47–50) (Supplemental Figure 1).

Construction of recombinant viruses. Recombinant virus UL13KM (YK405), encoding an enzymatically inactive UL13 mutant in which lysine at UL13 residue 176 was replaced with methionine (K176M) (Supplemental Figure 1), was generated by cotransfection of rabbit skin cells with ΔUL13 (R7356) DNA purified as described previously (51) and pUL13KM containing a 5.1-kbp *Afl*III fragment of HSV-1(F) DNA containing genes UL12, UL13, UL14, and part of UL15, with a K176M mutation in UL13 as described previously (18). UL13R (YK406) in which the K176M mutation in UL13KM was repaired (Supplemental Figure 1) was generated by cotransfection of rabbit skin cells with UL13KM (YK405) DNA and *Afl*III Pst+ in pBSΔV-Kp (18) containing the 5.1-kbp *Afl*III fragment of HSV-1(F) DNA into which a silent mutation in the wobble base of glutamine at position 219 of UL13 was introduced to create a *Pst*I restriction site as described previously (18). Plaques were isolated, purified, and screened for the presence of a *Pst*I site in the UL13 locus. Recombinant virus ΔUL41R (YK477) in which the UL41-null mutation was repaired was generated by the Red-mediated mutagenesis procedure as described previously (49). The genotype of each recombinant virus was confirmed by sequencing.

UL13KM (YK405) grew as well as WT HSV-1(F) and UL13R (YK406) in Vero cells at an MOI of 5 or 0.01 (Supplemental Figure 6, C and D). In contrast, growth of UL13KM (YK405) in rabbit skin cells was slightly reduced at both MOIs compared with growth of WT HSV-1(F) and UL13R (YK406) (Supplemental Figure 6, E and F). These results for UL13KM (YK405) were in agreement with those of another UL13 kinase-dead mutant virus as reported previously (18). Furthermore, the level of cellular β-actin mRNA in B6MEFs and Neuro-2a cells infected with UL13KM (YK405) was similar to that in cells infected with WT HSV-1(F) or UL13R (YK406) (Supplemental Figure 6, A and B). In contrast, in agreement with a previous report (8, 52), the level of β-actin mRNA in these cells infected with ΔUL41 (YK476) was significantly upregulated compared with that in cells infected with WT HSV-1(F) or ΔUL41R (YK477) (Supplemental Figure 6, A and B). UL41 encodes the HSV-1 vhs protein, which has endoribonuclease activity for the degradation of cellular mRNAs in HSV-1–infected cells. These results indicated that the kinase-dead mutation in UL13 had no effect on vhs activity in infected cells.

Detection of antigen presentation in infected cells. B6MEFs were grown in 24-well plates and infected with each of the indicated viruses at an MOI of 1. At 12 hours after infection, 1×10^5 HSV-2.3.2E2 cells were added to each well, and incubation was continued for an additional 12 hours. LacZ expression was then assayed as described previously (8).

Generation of Cxcl9-knockout mice by the CRISPR/Cas system. *Cxcl9*-deficient mice were generated by the offset-nicking method of the CRISPR/Cas system according to a previous report (28). Briefly, gRNAs for offset-nicking were designed at the following loci in *Cxcl9* exon2: 5′-TTATCACTAGGGTTCCTAGGCGG and 5′-TCCTGCATCAGCACCAGCCGAGG (underline indicates protospacer adjacent motif [PAM] site). Approximately 4 pl RNA solution, which contained 100 ng/μl *Cas9*^{D10A} mRNA and 10 ng/μl of each gRNA, was injected into the cytoplasm of each zygote obtained from naturally mated ICR female mice. After microinjection, all zygotes were cultured in M16 medium, and the 2-cell embryos were transferred into the oviducts of 0.5 days post-coitum (dpc) pseudopregnant recipient mice. After the pups' birth, genome DNA was extracted from the tail tips and subjected to PCR using the following primers: 5′-TGGAGGTTTTCTCTTCTTCCAAGG-3′ and 5′-TGTCCAGGTTCCTACACTCTCAG-3′. The genotype of each PCR product was confirmed by sequencing (Supplemental Figure 5A). The male pup harboring the mutation was mated to ICR female mice and tested for the germline transmission. To generate homozygotic *Cxcl9*-knockout ICR mice or WT mice, which were used as a control in the *Cxcl9*-knockout ICR experiment, each male or female mouse heterozygous for the deleted *Cxcl9* locus was crossed to heterozygous mice. Homozygous *Cxcl9*-knockout mice or WT mice were maintained and used for animal studies.

Primary MEFs. To isolate primary MEFs, 16 dpc embryos from either WT or *Cxcl9*-knockout ICR mice were cut into small pieces, incubated in 0.25% trypsin/1 mM EDTA (Wako) and 15 μg DNase I (Roche)/ml for 20 minutes at 37°C, then filtered through a 70-μm-pore-size filter. The cell suspension was cultured in DMEM supplemented with 10% FCS.

Animal studies. Female ICR mice were purchased from Charles River. For ocular infection, 5-week-old female mice were infected with 1×10^6 PFU UL13KM or UL13R per eye as described previously (53). Survival was monitored daily from 1 to 14 or 21 days after infection. To analyze virus antigen and/or titers in infected mouse brains, 5-week-old female mice were infected ocularly with 1×10^6 PFU of each of the indicated viruses per eye as described above. At the indicated times after infection, mice were sacrificed, and whole brains, eyes, and TGs were removed. Virus antigen in the brains and virus titers in the brains, eyes, and TGs of these mice were analyzed as described previously (50, 54).

Histopathology and immunohistochemistry. Brains from infected mice were perfused with 4% phosphate-buffered paraformaldehyde overnight at 4°C and then rinsed with 70% ethanol. The fixed brains were embedded in paraffin, sectioned, and stained with hematoxylin. Immunohistochemical detection of HSV-1 antigens was performed on paraffin-embedded sections as described previously (50). For immunohistochemical detection of other HSV-1 antigens, brains from infected mice were fixed with 4% phosphate-buffered paraformaldehyde overnight at 4°C; washed with PBS; and immersed in 5% sucrose in PBS for 1 hour, then in 15% sucrose in PBS for 3 hours, and finally in 30% sucrose in PBS overnight at 4°C. Brains were then embedded in OCT (Sakura), snap frozen in liquid nitrogen, and sectioned. The frozen sections were blocked with TNB buffer (0.5% TSA Blocking Reagent, PerkinElmer; 0.1 M Tris-HCl [pH 7.5] and 0.15 M NaCl) containing 5% normal donkey serum. To block endogenous biotin, the sections were further treated with an Avidin/Biotin Blocking Kit (Vector Laboratories), and endogenous peroxidase activity was quenched with 1% H_2O_2. The sections were stained with anti–HSV-1 antibody (B0114, Dako) overnight at 4°C, washed with PBS containing 0.05% Tween 20, and incubated with biotin-conjugated donkey F(ab′)$_2$ anti-rabbit IgG (711-066-152, Jackson ImmunoResearch Laboratories Inc.), followed by incubation with streptavidin-HRP conjugate (Zymed Laboratories). The antigens were detected using tyramide-fluorescein (PerkinElmer) according to the manufacturer's instructions. All sections were then counterstained with DAPI (Sigma-Aldrich) and mounted with Perma-Fluor Aqueous Mounting Medium (Thermo Scientific). The stained sections were analyzed using a fluorescence IX71 microscope equipped with a digital DP80 camera and CellSens software (Olympus).

Depletion of CD8$^+$ or CD4$^+$ T cells in mice. A dose of 200 μg anti-CD8α (53.6-72, ATCC) antibody or anti-CD4 (GK1.5, ATCC) antibody was administered to 5-week-old female ICR mice by intraperitoneal injection 2 days before HSV-1 infection. Administration of each antibody dose into mice routinely resulted in >95% depletion of CD8$^+$ or

$CD4^+$ cells in lymph node and spleen (data not shown). $CD8^+$ or $CD4^+$ cell depletion was maintained by repeated injections of monoclonal anti-CD8α or anti-CD4 antibody at 3-day intervals. Mice depleted of $CD8^+$ or $CD4^+$ T cells were ocularly infected with 1×10^6 PFU UL13KM or UL13R per eye, survival was monitored, and virus antigen and titers were analyzed as described above.

Injection of CXCL9 or CXCL10 into the brain stems of mice. Five-week-old female mice were infected ocularly with 1×10^6 PFU UL13KM or UL13R per eye as described above. At 5 days after infection, mice were anesthetized, their heads were shaved, and they were mounted into a stereotaxic Model 900M apparatus (DKI). The scalp was cut to reveal the skull, and two holes were drilled into the skull. To target the HSV-1–infected brain stems, Hamilton syringe needles were targeted to −0.32 cm (posterior) and ±0.20 cm (lateral) relative to bregma, and +0.30 cm (medial) relative to the skull. A total of 2 μl of a solution of 200 μg murine recombinant CXCL9 or CXCL10/ml (Peprotech) in PBS or 2 μl PBS was delivered over a 2-minute period, followed by a 2-minute rest. Needles were removed, and the scalp incision was closed with thread.

Flow cytometry. Five-week-old female mice were mock-infected or infected ocularly with 1×10^6 PFU UL13KM or UL13R per eye as described above. At the indicated times after infection, mice were sacrificed, and white blood cells in submandibular lymph nodes and/or spleens were isolated as described previously (8). For isolation of white blood cells in brain stems, eyes, or TGs, each tissue from infected mice was cut into small pieces; incubated in RPMI 1640 containing 2% fetal calf serum, 1 mg collagenase D/ml (Wako), and 15 μg DNase I (Roche)/ml for 30 minutes at 37°C; filtered through a 70-μm-pore-size filter; suspended in 15 ml 30% Percoll (GE Healthcare) in RPMI 1640; and centrifuged at 7,800 *g* for 30 minutes at room temperature (55). The myelin debris at the top of the brain stem or TG samples was removed, and the layer containing white blood cells above the red blood cell layer was collected and washed. The total number of viable white blood cells was determined by the trypan blue exclusion test. The isolated white blood cells were stained with FITC-conjugated anti-CD8α (53.6-72; eBioscience) and APC-conjugated anti-CD3ε (145-2C11; eBioscience) antibodies, or APC-conjugated anti-CD3ε (145-2C11; eBioscience) and PE-conjugated anti-CD45 (30-F11; eBioscience) antibodies in combination with PE-Cy7–conjugated anti-CD8α (53.6-72; BD) and FITC-conjugated anti-CD4 (GK1.5; BD) antibodies at 4°C for 30 minutes. Immediately before flow cytometry analysis, 7-amino-actinomycin D (7-AAD; BD) was added to the cells, and 7-AAD^+ dead cells were excluded from analysis. Multiparameter analyses were performed with a flow cytometer (Verse; BD). The total number of $CD8^+$ T cells per brain stem, eye, TG, or submandibular lymph node was calculated by multiplying the fraction of $CD45^+$ $CD3^+CD8\alpha^+$ cells (i.e., the number of $CD45^+CD3^+CD8\alpha^+$ cells divided by the number of viable 7-AAD^- cells) by the total number of viable white blood cells isolated per brain stem, eye, TG, or submandibular lymph node, respectively. The total number of $CD4^+$ T cells per brain stem, eye, TG, or submandibular lymph node was calculated by multiplying the fraction of $CD45^+CD3^+CD4^+$ cells (i.e., the number of $CD45^+CD3^+CD4^+$ cells divided by the number of viable 7-AAD^- cells) by the total number of viable white blood cells isolated per brain stem, eye, TG, or submandibular lymph node, respectively.

ELISPOT assays. Five-week-old female mice were infected ocularly with 1×10^6 PFU UL13KM or UL13R per eye as described above. At 7 days after infection, $CD8^+$ T cells were purified from white blood cells isolated from submandibular lymph nodes and brain stems of infected mice as described above using anti-CD8 microbeads (Miltenyi Biotec) according to the manufacturer's instructions. The purified cells routinely contained >80% $CD8^+$ T cells ($CD45^+$, $CD3^+$, $CD8\alpha^+$). The $CD8^+$ T cells were incubated with irradiated normal splenocytes (2×10^5 cells/well) that had been preincubated with or without heat-inactivated HSV-1(F) antigen (equivalent to 2×10^6 PFU/well) for 1 hour at 37°C, in 96-well PVDF Membrane ELISPOT plates (Millipore) that were precoated with anti–mouse IFN-γ Ab (AN-18; eBioscience) for 72 hours as described previously (56). The plates were developed with anti–mouse IFN-γ mAb (R4-6A2; eBioscience) according to the manufacturer's instructions (eBioscience) as described previously (56). The total number of HSV-1–specific IFN-γ–producing $CD8^+$ T cells per brain stem or submandibular lymph node was calculated by subtracting the number of IFN-γ–producing cells in wells without antigen from that in wells with HSV-1 antigens, and multiplying by the total number of $CD8^+$ T cells isolated per brain stem or submandibular lymph node.

Quantitative RT-PCR. Total RNA from infected cells in cell cultures was isolated with a High Pure RNA Isolation Kit (Roche) according to the manufacturer's instructions. For isolation of total RNA from brain stems in mice, mice that were mock-infected or infected with UL13KM or UL13R were sacrificed at the indicated times after infection. Brain stems from mock-infected and infected mice were homogenized in TriPure Isolation Reagent (Roche) using a Disposable Pestle System (Fisher), and total RNA was then isolated with a High Pure RNA Tissue Kit (Roche) according to the manufacturer's instructions. cDNA was synthesized from the isolated RNA with a Transcriptor First Strand cDNA Synthesis Kit (Roche) according to the manufacturer's instructions. The amount of cDNA of specific genes was quantitated using the Universal ProbeLibrary (Roche) with TaqMan Master (Roche) and the LightCycler 96 System (Roche) according to the manufacturer's instructions. Gene-specific primers and universal probes were designed using ProbeFinder software (Roche). The primer and probe sequences for mouse β-actin were 5′-GGAGGGGGTTGAGGTGTT-3′, 5′-GTGTGCACTTTTATTGGTCTCAA-3′, and Universal ProbeLibrary probe 71; for mouse *Il-6*, 5′-GCTACCAAACTGGATATAATCAGGA-3′, 5′-CCAGGTAGCTATGGTACTCCAGAA-3′, and Universal ProbeLibrary probe 6; for mouse *Cxcl9*, 5′-TGCTAGAGGCAAAAACTCTGTG-3′, 5′-TAGGCTCAAGGGCGTGAT-3′, and Universal ProbeLibrary probe 76; for mouse *Cxcl10*, 5′-CCTTGGTCTTCTGAAAGGTGAC-3′, 5′-ACCATGGCTTGACCATCATC-3′, and ProbeLibrary Probe 63; for mouse *Cxcl11*, 5′-GCTGCTGAGATGAACAGGAA-3′, 5′-CCCTGTTTGAACATAAGGAAGC-3′, and ProbeLibrary Probe 76; and for 18S rRNA, 5′-GCAATTATTCCCCATGAACG-3′, 5′-GGGACTTAATCAACGCAAGC-3′, and ProbeLibrary Probe 48. The amount of expression of each mRNA was normalized to the amount of expression of 18S rRNA. The relative amount of expression of each gene in the brain stem was calculated using the relative standard curve method. The relative amount of expression of each gene in cell culture was calculated using the comparative CT ($2^{-\Delta\Delta Ct}$) method (57).

Immunoblotting. Primary MEFs from WT or *Cxcl9*-knockout mice were mock-treated or treated with 20 ng/ml recombinant mouse IFN-γ (Peprotech). Cells were harvested at 18 hours after incubation and analyzed by immunoblotting as described previously (51) with recombinant mouse CXCL9 (Peprotech) as a control. Goat polyclonal antibody to CXCL9 (AF-492-NA; R&D Systems), mouse monoclonal antibody

to β-actin (AC15; Sigma-Aldrich), donkey anti-goat IgG-HRP (sc-2020; Santa Cruz Biotechnology Inc.), and sheep anti-mouse IgG, HRP-linked F(ab′)$_2$ fragment (NA9310; GE) were used for immunoblotting.

Statistics. Differences in β-actin mRNA amounts and antigen presentation were statistically analyzed by 1-way ANOVA followed by Tukey's post-test. Differences in survival of infected mice were statistically analyzed by the log-rank test. Differences in other data were statistically analyzed by the Mann–Whitney *U* test. A *P* value of 0.05 or less was considered statistically significant.

Study approval. All animal experiments were carried out in accordance with the Guidelines for Proper Conduct of Animal Experiments, Science Council of Japan. The protocol was approved by the IACUC of the Institute of Medical Science, University of Tokyo (IACUC protocol approval number: 19-26, PA11-81, PH12-10, PA15-14, and PA16-76).

Author contributions

NK conceived, designed, and performed the experiments, analyzed the data, and wrote the manuscript. T. Imai, KS, WF, SK, YM, JA, and AK assisted with the experiments and analyzed the data. AS, T. Ichinohe, NT, SU, and HK provided materials, assisted with the experiments, and analyzed the data. YK conceived and designed the experiments, analyzed the data, and wrote the manuscript.

Acknowledgments

We thank Tomoko Ando, Yoshie Asakura, Michiko Tanaka, and Ken Sagou for excellent technical assistance and/or sharing their reagents with us. This study was supported by the Funding Program for Next Generation World-Leading Researchers and Grants for Scientific Research from the Japan Society for the Promotion of Science (JSPS); grants for Scientific Research on Innovative Areas from the Ministry of Education, Culture, Science, Sports, and Technology (MEXT) of Japan (16H06433, 16H06429, 16K21723); a contract research fund for the Program of Japan Initiative for Global Research Network on Infectious Diseases (J-GRID) from MEXT and the Japan Agency for Medical Research and Development (AMED); and grants from the Takeda Science Foundation and the Mitsubishi Foundation.

Address correspondence to: Yasushi Kawaguchi, 4-6-1 Shirokanedai, Minato-ku, Tokyo 108-8639, Japan. Phone: 81.3.6409.2070; Email: ykawagu@ims.u-tokyo.ac.jp.

1. Roizman B, Knipe DM, Whitley RJ. In: Knipe DM, Howley PM, Cohen JI, Griffin DE, Lamb RA, Martin MA, et al, eds. *Fields Virology.* 6th ed. Philadelphia, Pennsylvania, USA: Lippincott Williams & Wilkins; 2013:1823–1897.
2. Whitley RJ, Gnann JW. Viral encephalitis: familiar infections and emerging pathogens. *Lancet*. 2002;359(9305):507–513.
3. Hansen TH, Bouvier M. MHC class I antigen presentation: learning from viral evasion strategies. *Nat Rev Immunol*. 2009;9(7):503–513.
4. Horst D, Verweij MC, Davison AJ, Ressing ME, Wiertz EJ. Viral evasion of T cell immunity: ancient mechanisms offering new applications. *Curr Opin Immunol*. 2011;23(1):96–103.
5. York IA, Roop C, Andrews DW, Riddell SR, Graham FL, Johnson DC. A cytosolic herpes simplex virus protein inhibits antigen presentation to CD8+ T lymphocytes. *Cell*. 1994;77(4):525–535.
6. Früh K, et al. A viral inhibitor of peptide transporters for antigen presentation. *Nature*. 1995;375(6530):415–418.
7. Hill A, et al. Herpes simplex virus turns off the TAP to evade host immunity. *Nature*. 1995;375(6530):411–415.
8. Imai T, et al. Us3 kinase encoded by herpes simplex virus 1 mediates downregulation of cell surface major histocompatibility complex class I and evasion of CD8+ T cells. *PLoS ONE*. 2013;8(8):e72050.
9. Ahn K, et al. Molecular mechanism and species specificity of TAP inhibition by herpes simplex virus ICP47. *EMBO J*. 1996;15(13):3247–3255.
10. Lang A, Nikolich-Zugich J. Development and migration of protective CD8+ T cells into the nervous system following ocular herpes simplex virus-1 infection. *J Immunol*. 2005;174(5):2919–2925.
11. Coulter LJ, Moss HW, Lang J, McGeoch DJ. A mutant of herpes simplex virus type 1 in which the UL13 protein kinase gene is disrupted. *J Gen Virol*. 1993;74(Pt 3):387–395.
12. Purves FC, Ogle WO, Roizman B. Processing of the herpes simplex virus regulatory protein alpha 22 mediated by the UL13 protein kinase determines the accumulation of a subset of alpha and gamma mRNAs and proteins in infected cells. *Proc Natl Acad Sci U S A*. 1993;90(14):6701–6705.
13. Kawaguchi Y, Kato K, Tanaka M, Kanamori M, Nishiyama Y, Yamanashi Y. Conserved protein kinases encoded by herpesviruses and cellular protein kinase cdc2 target the same phosphorylation site in eukaryotic elongation factor 1delta. *J Virol*. 2003;77(4):2359–2368.
14. Kudoh A, et al. Phosphorylation of MCM4 at sites inactivating DNA helicase activity of the MCM4-MCM6-MCM7 complex during Epstein-Barr virus productive replication. *J Virol*. 2006;80(20):10064–10072.
15. Hume AJ, Finkel JS, Kamil JP, Coen DM, Culbertson MR, Kalejta RF. Phosphorylation of retinoblastoma protein by viral protein with cyclin-dependent kinase function. *Science*. 2008;320(5877):797–799.
16. Van Sant C, Kawaguchi Y, Roizman B. A single amino acid substitution in the cyclin D binding domain of the infected cell protein no. 0 abrogates the neuroinvasiveness of herpes simplex virus without affecting its ability to replicate. *Proc Natl Acad Sci U S A*. 1999;96(14):8184–8189.
17. Kastrukoff LF, Lau AS, Puterman ML. Genetics of natural resistance to herpes simplex virus type 1 latent infection of the peripheral nervous system in mice. *J Gen Virol*. 1986;67(Pt 4):613–621.
18. Tanaka M, Nishiyama Y, Sata T, Kawaguchi Y. The role of protein kinase activity expressed by the UL13 gene of herpes simplex virus 1: the activity is not essential for optimal expression of UL41 and ICP0. *Virology*. 2005;341(2):301–312.
19. Lundberg P, et al. The immune response to herpes simplex virus type 1 infection in susceptible mice is a major cause of central nervous system pathology resulting in fatal encephalitis. *J Virol*. 2008;82(14):7078–7088.
20. Mueller SN, Jones CM, Smith CM, Heath WR, Carbone FR. Rapid cytotoxic T lymphocyte activation occurs in the draining lymph nodes after cutaneous herpes simplex virus infection as a result of early antigen presentation and not the presence of virus. *J Exp Med*. 2002;195(5):651–656.
21. Groom JR, Luster AD. CXCR3 ligands: redundant, collaborative and antagonistic functions. *Immunol Cell Biol*. 2011;89(2):207–215.
22. Shin H, Iwasaki A. A vaccine strategy that protects against genital herpes by establishing local memory T cells. *Nature*. 2012;491(7424):463–467.
23. Wuest T, Farber J, Luster A, Carr DJ. CD4+ T cell migration into the cornea is reduced in CXCL9 deficient but not CXCL10 deficient mice following herpes simplex virus type 1 infection. *Cell Immunol*. 2006;243(2):83–89.
24. Moir S, et al. Evidence for HIV-associated B cell exhaustion in a dysfunctional memory B cell compartment in HIV-infected viremic individuals. *J Exp Med*. 2008;205(8):1797–1805.
25. Hartl D, et al. Infiltrated neutrophils acquire novel chemokine receptor expression and chemokine responsiveness in chronic inflammatory lung diseases. *J Immunol*. 2008;181(11):8053–8067.
26. Biber K, Dijkstra I, Trebst C, De Groot CJ, Ransohoff RM, Boddeke HW. Functional expression of CXCR3 in cultured mouse and human astrocytes and microglia. *Neuroscience*. 2002;112(3):487–497.
27. Xia MQ, Bacskai BJ, Knowles RB, Qin SX, Hyman BT. Expression of the chemokine receptor CXCR3 on neurons and the elevated expression of its ligand IP-10 in reactive astrocytes: in vitro ERK1/2 activation and role in Alzheimer's disease. *J Neuroimmunol*. 2000;108(1–2):227–235.
28. Fujii W, Onuma A, Sugiura K, Naito K. Efficient generation of genome-modified mice via offset-nicking by CRISPR/Cas system. *Biochem Biophys Res Commun*. 2014;445(4):791–794.
29. Anglen CS, Truckenmiller ME, Schell TD, Bonneau RH. The dual role of CD8+ T lymphocytes in the development of stress-induced herpes simplex encephalitis. *J Neuroimmunol*. 2003;140(1–2):13–27.

30. Hosking MP, Lane TE. The role of chemokines during viral infection of the CNS. *PLoS Pathog*. 2010;6(7):e1000937.
31. Alcami A. Viral mimicry of cytokines, chemokines and their receptors. *Nat Rev Immunol*. 2003;3(1):36–50.
32. Kramer T, Enquist LW. Directional spread of alphaherpesviruses in the nervous system. *Viruses*. 2013;5(2):678–707.
33. Ghiasi H, Cai S, Perng GC, Nesburn AB, Wechsler SL. Both CD4+ and CD8+ T cells are involved in protection against HSV-1 induced corneal scarring. *Br J Ophthalmol*. 2000;84(4):408–412.
34. Rajasagi NK, Kassim SH, Kollias CM, Zhao X, Chervenak R, Jennings SR. CD4+ T cells are required for the priming of CD8+ T cells following infection with herpes simplex virus type 1. *J Virol*. 2009;83(10):5256–5268.
35. Kastrukoff LF, et al. Redundancy in the immune system restricts the spread of HSV-1 in the central nervous system (CNS) of C57BL/6 mice. *Virology*. 2010;400(2):248–258.
36. Frank GM, Lepisto AJ, Freeman ML, Sheridan BS, Cherpes TL, Hendricks RL. Early CD4(+) T cell help prevents partial CD8(+) T cell exhaustion and promotes maintenance of Herpes Simplex Virus 1 latency. *J Immunol*. 2010;184(1):277–286.
37. Asai R, Ohno T, Kato A, Kawaguchi Y. Identification of proteins directly phosphorylated by UL13 protein kinase from herpes simplex virus 1. *Microbes Infect*. 2007;9(12–13):1434–1438.
38. Kurt-Jones EA, et al. Herpes simplex virus 1 interaction with Toll-like receptor 2 contributes to lethal encephalitis. *Proc Natl Acad Sci U S A*. 2004;101(5):1315–1320.
39. Marques CP, Cheeran MC, Palmquist JM, Hu S, Urban SL, Lokensgard JR. Prolonged microglial cell activation and lymphocyte infiltration following experimental herpes encephalitis. *J Immunol*. 2008;181(9):6417–6426.
40. McCandless EE, Zhang B, Diamond MS, Klein RS. CXCR4 antagonism increases T cell trafficking in the central nervous system and improves survival from West Nile virus encephalitis. *Proc Natl Acad Sci U S A*. 2008;105(32):11270–11275.
41. Goverman J. Autoimmune T cell responses in the central nervous system. *Nat Rev Immunol*. 2009;9(6):393–407.
42. Moseman EA, McGavern DB. The great balancing act: regulation and fate of antiviral T-cell interactions. *Immunol Rev*. 2013;255(1):110–124.
43. Lundberg P, Openshaw H, Wang M, Yang HJ, Cantin E. Effects of CXCR3 signaling on development of fatal encephalitis and corneal and periocular skin disease in HSV-infected mice are mouse-strain dependent. *Invest Ophthalmol Vis Sci*. 2007;48(9):4162–4170.
44. Sun J, Madan R, Karp CL, Braciale TJ. Effector T cells control lung inflammation during acute influenza virus infection by producing IL-10. *Nat Med*. 2009;15(3):277–284.
45. Sun K, Torres L, Metzger DW. A detrimental effect of interleukin-10 on protective pulmonary humoral immunity during primary influenza A virus infection. *J Virol*. 2010;84(10):5007–5014.
46. Tanaka M, Kagawa H, Yamanashi Y, Sata T, Kawaguchi Y. Construction of an excisable bacterial artificial chromosome containing a full-length infectious clone of herpes simplex virus type 1: viruses reconstituted from the clone exhibit wild-type properties in vitro and in vivo. *J Virol*. 2003;77(2):1382–1391.
47. Ejercito PM, Kieff ED, Roizman B. Characterization of herpes simplex virus strains differing in their effects on social behaviour of infected cells. *J Gen Virol*. 1968;2(3):357–364.
48. Purves FC, Longnecker RM, Leader DP, Roizman B. Herpes simplex virus 1 protein kinase is encoded by open reading frame US3 which is not essential for virus growth in cell culture. *J Virol*. 1987;61(9):2896–2901.
49. Kato A, et al. Identification of a physiological phosphorylation site of the herpes simplex virus 1-encoded protein kinase Us3 which regulates its optimal catalytic activity in vitro and influences its function in infected cells. *J Virol*. 2008;82(13):6172–6189.
50. Tanaka M, et al. Herpes simplex virus 1 VP22 regulates translocation of multiple viral and cellular proteins and promotes neurovirulence. *J Virol*. 2012;86(9):5264–5277.
51. Kawaguchi Y, Van Sant C, Roizman B. Herpes simplex virus 1 alpha regulatory protein ICP0 interacts with and stabilizes the cell cycle regulator cyclin D3. *J Virol*. 1997;71(10):7328–7336.
52. Everly DN, Feng P, Mian IS, Read GS. mRNA degradation by the virion host shutoff (Vhs) protein of herpes simplex virus: genetic and biochemical evidence that Vhs is a nuclease. *J Virol*. 2002;76(17):8560–8571.
53. Sagou K, Imai T, Sagara H, Uema M, Kawaguchi Y. Regulation of the catalytic activity of herpes simplex virus 1 protein kinase Us3 by autophosphorylation and its role in pathogenesis. *J Virol*. 2009;83(11):5773–5783.
54. Koyanagi N, Imai T, Arii J, Kato A, Kawaguchi Y. Role of herpes simplex virus 1 Us3 in viral neuroinvasiveness. *Microbiol Immunol*. 2014;58(1):31–37.
55. Howe CL, et al. Hippocampal protection in mice with an attenuated inflammatory monocyte response to acute CNS picornavirus infection. *Sci Rep*. 2012;2:545.
56. Sato A, et al. Vaginal memory T cells induced by intranasal vaccination are critical for protective T cell recruitment and prevention of genital HSV-2 disease. *J Virol*. 2014;88(23):13699–13708.
57. Livak KJ, Schmittgen TD. Analysis of relative gene expression data using real-time quantitative PCR and the 2(-Delta Delta C(T)) Method. *Methods*. 2001;25(4):402–408.